Choroidal Hyper-Reflective Foci in Geographic Atrophy

Enrico Borrelli,[1,2] Michele Reibaldi,[3] Costanza Barresi,[1,2] Alessandro Berni,[1,2] Ugo Introini,[1,2] and Francesco Bandello[1,2]

[1]Vita-Salute San Raffaele University Milan, Milan, Italy
[2]IRCCS San Raffaele Scientific Institute, Milan, Italy
[3]Department of Ophthalmology, University of Turin, Turin, Italy

Correspondence: Enrico Borrelli, Department of Ophthalmology, University Vita-Salute San Raffaele, Via Olgettina 60, Milan, Italy; borrelli.enrico@yahoo.com.

Received: August 16, 2023
Accepted: October 17, 2023
Published: November 3, 2023

Citation: Borrelli E, Reibaldi M, Barresi C, Berni A, Introini U, Bandello F. Choroidal hyper-reflective foci in geographic atrophy. *Invest Ophthalmol Vis Sci.* 2023;64(14):5. https://doi.org/10.1167/iovs.64.14.5

Purpose. The purpose of this study was to describe the presence of choroidal hyper-reflective foci (HRF) on optical coherence tomography (OCT) in patients with geographic atrophy (GA). The relationship between the presence and quantity of choroidal HRF and other clinical and imaging factors was also investigated.

Methods. A total of 40 participants (40 eyes) with GA and age-related macular degeneration (AMD) were retrospectively analyzed. OCT images were reviewed for the presence, characteristics, and localization of choroidal HRF. The amount of choroidal HRF was quantified in different choroidal layers by two different (i.e. threshold reflectivity and manual counting) methodologies. The primary outcome was to describe and quantify choroidal HRF and correlate them with GA lesion size.

Results. Structural OCT images showed that all patients had multiple hyper-reflective deposits in different layers of the choroid. These hyper-reflective deposits in the choroid were located near Bruch's membrane or the edges of the blood vessels, particularly in the Sattler's layer, and none were observed inside the vessels. Choroidal HRF exhibited variable size and shape and varying effects on the posterior signal, including shadowing or hypertransmission. Mean ± SD number of choroidal HRF per B-scan was 21.5 ± 15.4 using the threshold reflectivity methodology and 25.1 ± 16.0 using the manual counting methodology. A significant correlation between the untransformed GA size and number of HRF was found, considering both quantitative strategies.

Conclusions. Hyper-reflective dots in the choroid of subjects with GA may be readily identified with structural OCT. These HRF might represent a natural component of the choroid that becomes more visible due to the absence of the retinal pigment epithelium.

Keywords: age-related macular degeneration (AMD), choroid, optical coherence tomography (OCT)

Geographic atrophy (GA) is the non-neovascular form of late age-related macular degeneration (AMD).[1] GA prevalence increases exponentially with age[2] and it is estimated to be responsible for 10 to 20% of cases of legal blindness in patients with AMD.[3] The exact causes of AMD are not fully understood, but GA is primarily characterized by the degeneration of the outer retina, the retinal pigment epithelium (RPE), and the choriocapillaris (CC).[4]

Structural optical coherence tomography (OCT) is an essential diagnostic tool for assessing individuals with GA, as it provides valuable anatomic information about the neuroretina, RPE, and choroid. The use of structural OCT has greatly expanded our understanding of GA, and studies utilizing this imaging technique have identified several biomarkers that are associated with the occurrence and progression of GA. These biomarkers include the size, volume, and subtype of drusen, the presence of neuroretinal hyper-reflective foci (HRF), thin double-layer sign, and subretinal drusenoid deposits (i.e. also known as reticular pseudodrusen [RPD]), thinning of the outer retina, degradation of photoreceptors, choroidal thinning, and CC loss.[4–11]

Using spectral domain OCT, neuroretinal HRF were first described by Coscas et al.[12] in 2009 in patients with exudative neovascular AMD. These OCT findings are typically visualized as oval- or round-shaped well-circumscribed hyper-reflective lesions within the neuroretina.[13–15] These lesions are required to have a reflectivity that is equal to or greater than that of the RPE layer.[13–15] Over the last years, several authors have sought to elucidate the significance and origin of these lesions in several retinal and choroidal disorders through histologic and advanced retinal imaging studies.

In AMD, neuroretinal HRF have been proposed to originate from activated RPE cells that migrate within the retina.[16] Alternatively, it was demonstrated that retinal melanophages are also responsible for the emergence of neuroretinal HRF in cases of AMD.[17] Additionally, neuroretinal HRF may serve as precursors of type 3 macular neovascularization (MNV).[18] Using structural OCT, previous studies have found that the amount of HRF is associated with disease stage in AMD.[19]

Moreover, as mentioned above, the presence and amount of neuroretinal HRF is associated with GA occurrence and progression. In detail, Nassisi et al.[13] retrospectively investigated 501 early/intermediate AMD eyes of 501 patients with unilateral MNV. They demonstrated that the presence of neuroretinal HRF was significantly associated with the development of late AMD at month 24. Importantly, this correlation remained significant when the authors considered only the progression to GA and MNV alone, the latter finding suggesting that presence of HRF is a consistent risk factor for the development of GA. In another study, the amount of neuroretinal HRF was measured using structural OCT and a significant association between number of HRF and progression to GA was displayed.[14] Finally, Schmidt-Erfurth and colleagues[20] prospectively enrolled 54 patients (87 eyes) with GA who were assessed using structural OCT for a median follow-up of 28 months. They demonstrated that the local GA progression speed was positively correlated with local increase of HRF.

Choroidal HRF have recently been captured with structural OCT imaging in different disorders, including diabetic macular edema[21] and Stargardt disease.[22] These OCT observations were identified in all of the choroidal layers and were predominantly situated within the choroidal stroma. After observing the presence of choroidal hyperreflective foci on structural OCT in patients with GA secondary to AMD, we conducted a study that aimed to comprehensively analyze these OCT features in GA. Notably, we examined the relationship between the presence and quantity of choroidal HRF and other clinical and imaging factors. Significantly, the quantification of choroidal HRF was conducted through both manual and automated methods.

Methods

This study adhered to the 1964 Helsinki declaration and its later amendments. All patients involved signed an informed consensus form approved by the local ethics committee.

Subjects

Forty consecutive patients with GA secondary to AMD[23] were selected from the medical records at San Raffaele Scientific institute in the period between January 2022 and December 2022. At the baseline visit, the following exclusion criteria were considered for the study eye: (i) medical history or evidence of MNV, including nonexudative cases; (ii) history of retinal surgery including antivascular endothelial growth factor (VEGF) injections; and (iii) history or evidence of other retinal and optic nerve disorders. Furthermore, we excluded eyes with an exceptionally thin choroid that made it challenging to differentiate between the choroidal layers during the analysis.

Structural OCT was performed with the Heidelberg Spectralis HRA + OCT device (Heidelberg Engineering, Heidelberg, Germany). The spectral domain OCT imaging session included 19 horizontal B-scans covering approximately a 5.5 × 4.5-mm area centered on the fovea. Each B-scan was composed of 25 averaged OCT images. A minimum signal strength of 25 was required to the OCT images to be included, as recommended by the manufacturer.[24]

A group of 15 patients (15 eyes) with intermediate AMD[25] was also included for comparisons. In these patients, the manual counting methodology was used to define the presence and amount of choroidal HRF.

OCT Grading

Structural OCT images were first reviewed for eligibility by an experienced and certified grader (author E.B.). We only analyzed volumetric scans in which the choroid was fully visible in all the B-scans.

Similar to Piri et al.,[22] who quantified choroidal HRF in Stargardt disease, prior to individually quantifying the choroidal HRF, the two graders reached a consensus on identifying and delineating each layer in the OCT sections. This grading was performed following the description by Zhao and colleagues.[26] Specifically, they defined Haller's layer as the outermost choroidal layer housing the large choroidal vessels. Sattler's layer was described as the region containing medium-sized choroidal vessels, which appeared as medium-sized, less intense spaces surrounded by a more intense stroma. The CC was characterized as the less reflective layer situated above Sattler's layer and encompassing Bruch's membrane as well. Therefore, eyes were independently graded for the presence and amount of HRF in the choroidal layers. The HRF were defined as round or oval areas with high reflectivity (i.e. black or white in color on white-over-black and black-over-white images, respectively), with a diameter between 10 and 50 µm.[22] Two observers (authors E.B. and C.B.) independently counted the number of HRF in different layers of the choroid, including the CC, Sattler's layer of the choroid, and Haller's layer of the choroid. The identification and counting were performed on a high-magnification white-over-black spectral domain OCT images, in order to improve the identification of HRF in the choroid, as previously suggested.[22] The values provided by both graders were utilized to evaluate the consistency between graders (i.e. intergrader repeatability). Conversely, the average of the ratings from the two graders was incorporated into the analysis. Last, one of the two referees conducted the grading process twice on different days to determine the consistency within their own assessments (i.e. intragrader repeatability).

The untransformed GA lesion size area (i.e. without square root transformation) was also measured using the built-in software caliper. In detail, the graders used a two-pronged approach for quantifying the GA area on near-infrared reflectance (NIR) images. First, they utilized the built-in software caliper to measure the regions displaying RPE atrophy, which appear as hyper-reflective areas in this imaging modality. Recognizing that subfoveal choroidal thickness might influence NIR intensity and potentially introduce variability across images,[27,28] they also incorporated structural OCT to enhance the visualization of areas with complete RPE and outer retina atrophy (cRORA).[29] To achieve more precise measurements, they meticulously examined OCT B-scans, scrolling through them to confirm the presence of hyper-reflective areas on NIR images that corresponded to regions of RPE atrophy.

For patients who had a follow-up visit at 1 year, the grading for choroidal HRF was performed in order to qualitatively assess any changes in the amount and location of HRF over time.

Image Processing to Obtain the Threshold Reflectivity Methodology

For each eye, OCT B-scan images from the volumetric scan were exported in PNG format and subsequently imported into the ImageJ software version 2.0 (National Institutes of Health, Bethesda, MD, USA; available at

Investigative Ophthalmology & Visual Science

http://rsb.info.nih.gov/ij/index.html) for image analysis. Each image was thus transformed in an 8-bit gray-scale image. Images were thus binarized using the local "Sauvola" threshold, in order to visualize choroidal HRF regardless of the presence of RPE atrophy. This approach was adopted to avoid overestimating HRF in regions with atrophy, as atrophy can cause hypertransmission signals into the choroid, making a general threshold inappropriate. The two graders confirmed these observations. Thresholded images were then used by one of the two graders (author E.B.) to determine the number and location of HRF within the choroid (Supplementary Fig. S1).

Statistical Analysis

Statistical calculations were performed using Statistical Package for Social Sciences (version 23.0.0.0; SPSS Inc., Chicago, IL, USA).

The analysis included descriptive statistics for demographics and main clinical data, and qualitative descriptions of the imaging characteristics. Moreover, the data were grouped according to the choroidal layer analyzed, and quantitative values were reported as mean ± standard deviation (SD) in the "Results" section and tables. Quantitative data were examined to assess their normal distribution. Friedman's two-way analysis of variance (ANOVA) non-parametric test was conducted to compare the number of choroidal HRF among the different choroidal layers. Independent-samples Mann-Whitney *U* test was used to compare the different groups.

Intergrader and intragrader repeatability were evaluated by computing the intraclass correlation coefficients (ICCs). The agreement between counting methodologies was investigated using Bland-Altman analysis. Moreover, Spearman's rank correlation coefficient (ρ) was calculated between the number of choroidal HRF obtained using the two counting methodologies.

Spearman's rank correlation coefficient was calculated between the number of choroidal HRF and untransformed GA size in order to determine whether HRF amount increases with the GA enlargement. Because multiple linear regression analysis allows us to estimate the association between a given dependent variable and other parameters, it provides a way of adjusting for (or accounting for) potentially confounding variables. Thus, subsequently, a multiple regression analysis with number of choroidal HRF as the dependent variable was applied, adjusting for age, gender, diabetes, and choroidal thickness.

Results

A total of 40 eyes from 40 Caucasian patients (21 female patients) with GA secondary to non-neovascular AMD were included in our analysis. Mean ± SD age was 72.3 ± 7.7 years. Overall, the best corrected visual acuity (BCVA) was 0.22 ± 0.17 LogMAR (Snellen VA of approximately 20/32). The untransformed GA area size was 1.75 ± 2.74 mm^2. Out of 40 eyes examined, 12 exhibited signs of subretinal drusenoid deposits, also referred to as reticular pseudodrusen. In addition, 11 of these eyes showed evidence of atrophy in the foveal region, and 12 displayed evidence of multifocal GA.

Presence, Localization, and Quantification of Choroidal Hyper-Reflective Foci

The examination of the structural OCT images showed that all patients had multiple hyper-reflective deposits in differ-

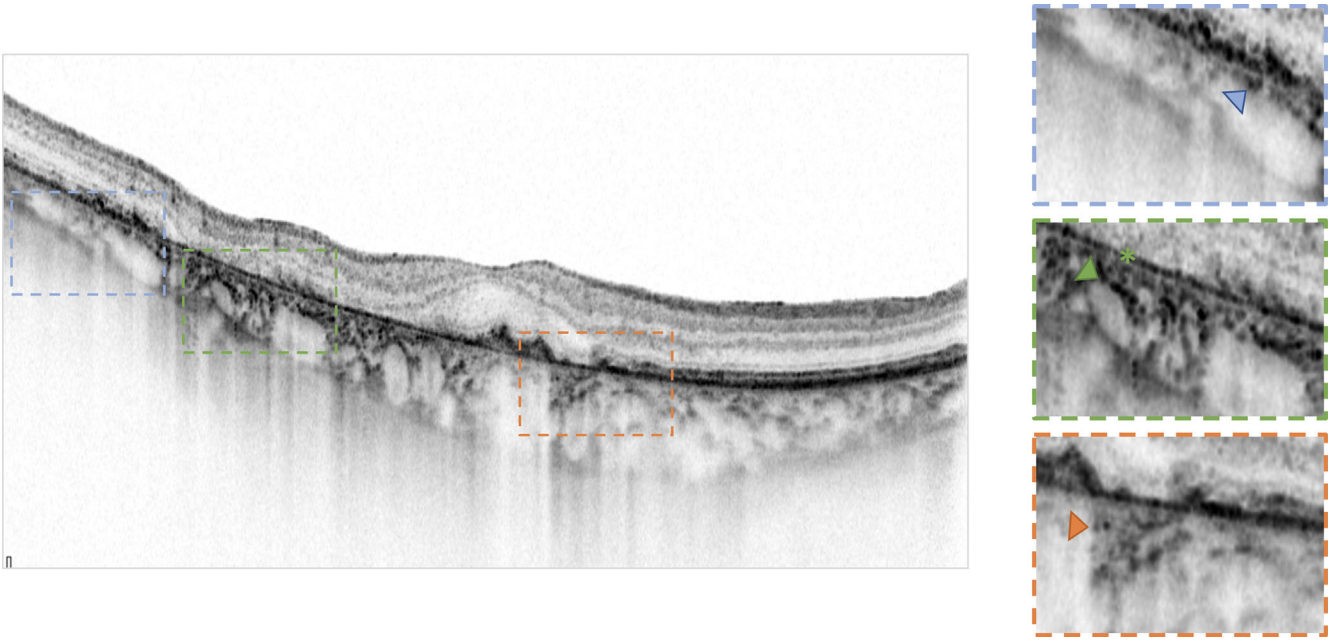

Figure 1. Representative optical coherence tomography (OCT) B-scan of a patient with geographic atrophy (GA). OCT B-scan (*left*) showing the presence of hyper-reflective foci (HRF) within the choroid. A magnified visualization of specific regions is reported in the right column. The structural OCT image shows multiple hyper-reflective deposits in different layers of the choroid, which mostly colocalize with regions with atrophy. These hyper-reflective deposits in the choroid were located near Bruch's membrane (*green asterisk*) or the edges of the blood vessels (*arrowheads*). The dimensions and shape of HRF showed significant variability, with a predominant smaller and round appearance near Bruch's membrane, whereas larger and *oval* shapes were observed in deeper layers.

Investigative Ophthalmology & Visual Science

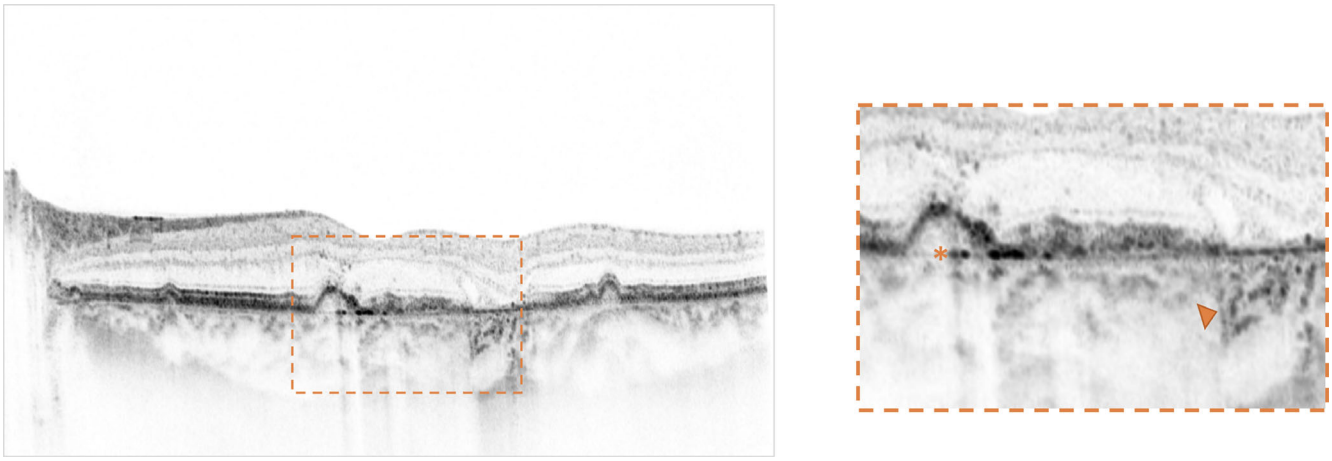

Figure 2. Representative optical coherence tomography (OCT) B-scan of a patient with geographic atrophy (GA). OCT B-scan (*left*) showing the presence of choroidal hyper-reflective foci (HRF). A magnified visualization of the foveal region is reported in the right column. Choroidal HRF are not limited to regions with retinal pigment epithelium (RPE) atrophy, as they were visualizable also in regions with conserved RPE (*orange asterisk*). Hyper-reflective deposits are localized near Bruch's membrane (*orange asterisk*) and within the choroidal stroma (*orange arrowhead*).

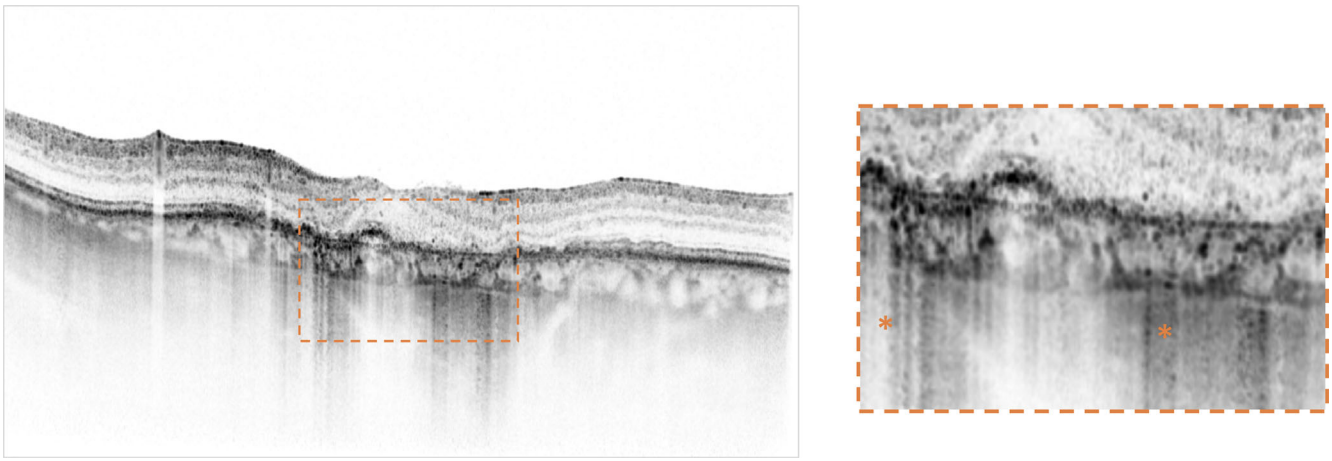

Figure 3. Representative optical coherence tomography (OCT) B-scan of a patient with geographic atrophy (GA). OCT B-scan (*left*) showing the presence of choroidal hyper-reflective foci (HRF). A magnified visualization of the foveal region is reported on the *right*. Hyper-reflective deposits are localized near Bruch's membrane (*orange asterisk*) and within the choroidal stroma (*orange arrowhead*). Choroidal HRF exhibited varying effects on the posterior signal, including shadowing or hypertransmission, the latter characteristic causing a barcode effect within the underlying sclera (*orange asterisks*).

ent layers of the choroid. These hyper-reflective deposits in the choroid were located near Bruch's membrane or the edges of the blood vessels, and none were observed inside the vessels (Fig. 1). A majority of the hyper-reflective deposits in the choroid were found in the same areas as regions with cRORA. The dimensions and shape of HRF showed significant variability, with a predominant smaller and round appearance near Bruch's membrane, whereas larger and oval shapes were observed in deeper layers (see Figs. 1, 2). Choroidal HRF exhibited varying effects on the posterior signal, including shadowing or hypertransmission (Fig. 3).

Mean ± SD number of choroidal HRF per B-scan was 21.5 ± 15.4 using the threshold reflectivity methodology and 25.1 ± 16.0 using the manual counting methodology (see the Table). Mean ± SD number of choroidal HRF in the entire OCT volume was 409.2 ± 292.7 and 476.0 ± 303.5 using the threshold reflectivity and manual counting methodologies, respectively (see the Table).

The Table summarizes the number of HRF in the different layers of the choroid. In details, using the threshold reflectivity methodology, mean ± SD number of choroidal HRF per B-scan differed between the layers ($P < 0.0001$): 11.7 ± 8.4 in the CC, 8.0 ± 5.8 in the Sattler's layer, and 1.9 ± 3.1 in the Haller's layer. Similarly, mean ± SD number of choroidal HRF in the entire OCT volume was 221.9 ± 159.9 in the CC, 151.9 ± 111.1 in the Sattler's layer, and 35.4 ± 59.5 in the Haller's layer ($P < 0.0001$). Values obtained using the manual counting methodology are reported in the Table.

In patients with intermediate AMD, mean ± SD number of choroidal HRF in the entire OCT volume was 17.3 ± 11.3 in the CC, 12.8 ± 8.2 in the Sattler's layer, 3.2 ± 4.5 in the Haller's layer, and 33.3 ± 21.2 considering the entire choroid ($P < 0.0001$ in all the comparisons with the GA group) Figure 4.

Investigative Ophthalmology & Visual Science

Table. Number of Choroidal Hyper-Reflective Foci Using Different Methodologies

	Threshold Reflectivity Methodology		Manual Counting Methodology	
	Number Per B-Scan	Number in the Entire OCT Volume	Number Per B-Scan	Number in the Entire OCT Volume
Choriocapillaris layer	11.7 ± 8.4	221.9 ± 159.9	13.0 ± 8.5	247.1 ± 161.9
Sattler's layer	8.0 ± 5.8	151.9 ± 111.1	9.6 ± 6.2	182.8 ± 117.5
Haller's layer	1.9 ± 3.1	35.4 ± 59.5	2.4 ± 3.4	46.0 ± 64.0
Whole choroid	21.5 ± 15.4	409.2 ± 292.7	25.1 ± 16.0	476.0 ± 303.5

Quantitative values are expressed in mean and SD (standard deviation)

Intergrader and Intragrader Repeatability for the Manual Counting

Considering the entire OCT volume, the intergrader repeatability was high for counting HRF in the CC (ICC = 0.798–0.999), Sattler's layer (ICC = 0.731–0.999), Haller's layer (ICC = 0.982–1.000), and the entire choroid (ICC = 0.786–0.999). Similarly, the intragrader repeatability was excellent for counting HRF in the CC (ICC = 0.968–1.000), Sattler's layer (ICC = 0.944–1.000), Haller's layer (ICC = 1.000–1.000), and the entire choroid (ICC = 0.919–1.000).

Agreement Between the Threshold Reflectivity and Manual Counting Methodologies

The Bland-Altman analysis showed a high agreement between the two methodologies to quantify the choroidal HRF (Supplementary Fig. S2). Considering the entire OCT volume, the mean absolute inter-method difference between measured choroidal HRF was 25.2, 30.9, 10.6, and 66.8 for CC, Sattler's layer, Haller's layer, and whole choroid, respectively. Similarly, considering the choroidal HRF number per B-scan, the mean absolute inter-method difference was 1.3 for CC, 1.6 for Sattler's layer, 0.6 for Haller's layer, and 3.5 for the whole choroid.

Bland-Altman findings were confirmed by Spearman's correlation analysis between values obtained considering the entire OCT volume ($\rho = 0.987$ and $P < 0.0001$ for CC, $\rho = 0.987$ and $P < 0.0001$ for Sattler's layer, $\rho = 0.860$ and $P < 0.0001$ for Haller's layer, and $\rho = 0.981$ and $P < 0.0001$ for the whole choroid), indicating a highly statistically significant correlation between the two different methodologies.

Association Between Amount of Choroidal Hyper-Reflective Foci in the OCT Volume and GA Size

Figure 5 shows the number of HRF in the different choroidal layers (i.e. considering the entire OCT volume) as a correlation of GA size. There was a significant correlation between the mean number of HRF in the CC ($\rho = 0.748$ and $P < 0.0001$ for threshold reflectivity methodology, $\rho = 0.727$ and $P < 0.0001$ for manual counting methodology, respectively), Sattler's layer ($\rho = 0.495$ and $P = 0.001$ for threshold reflectivity methodology, $\rho = 0.491$ and $P = 0.001$ for manual counting methodology, respectively), or Haller's layer ($\rho = 0.386$ and $P = 0.014$ for threshold reflectivity methodology, $\rho = -0.351$ and $P = 0.026$ for manual counting methodology, respectively) and untransformed GA area size. Similarly, there was a significant correlation between the untransformed GA size and number of HRF in the whole choroid considering both the threshold reflectivity ($\rho = 0.679$ and $P < 0.0001$) and manual counting ($\rho = 0.672$ and $P < 0.0001$) methodologies (Fig. 5).

In multiple regression analysis, the number of HRF in the whole choroid (i.e. dependent variable) was significantly associated with the untransformed GA size (standardized β coefficient = 0.768 and $P < 0.0001$), although no associations were found with the choroidal thickness ($P = 0.577$), gender ($P = 0.156$), and age ($P = 0.482$).

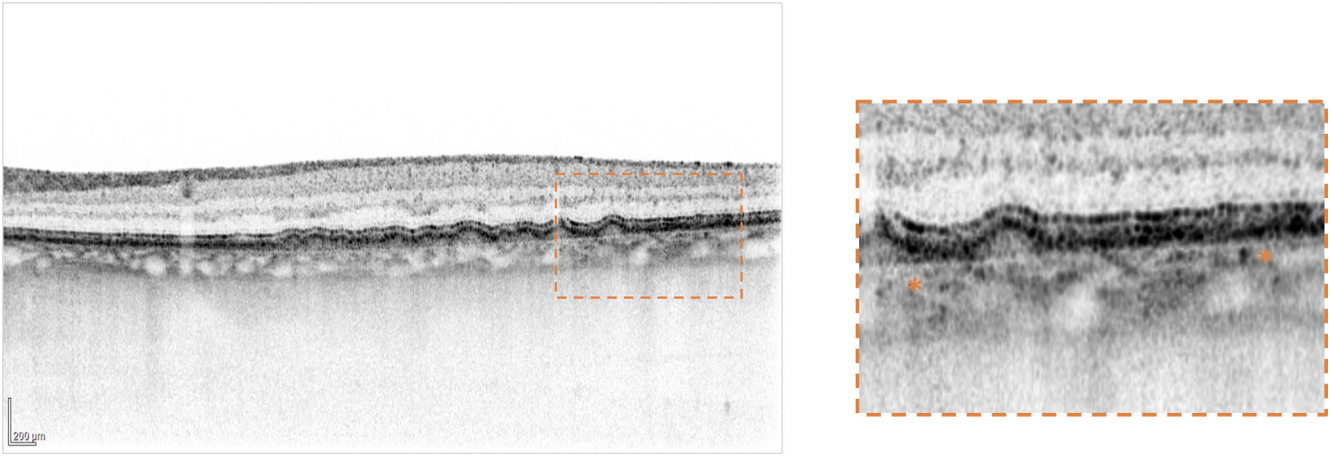

Figure 4. **Representative optical coherence tomography (OCT) B-scans of a patient with intermediate AMD.** OCT B-scans (*left*) showing the presence of choroidal hyper-reflective foci (HRF). A magnified visualization of the temporal region is reported on the right. Hyper-reflective deposits are localized near Bruch's membrane and within the choroidal stroma (*orange asterisks*).

Investigative Ophthalmology & Visual Science

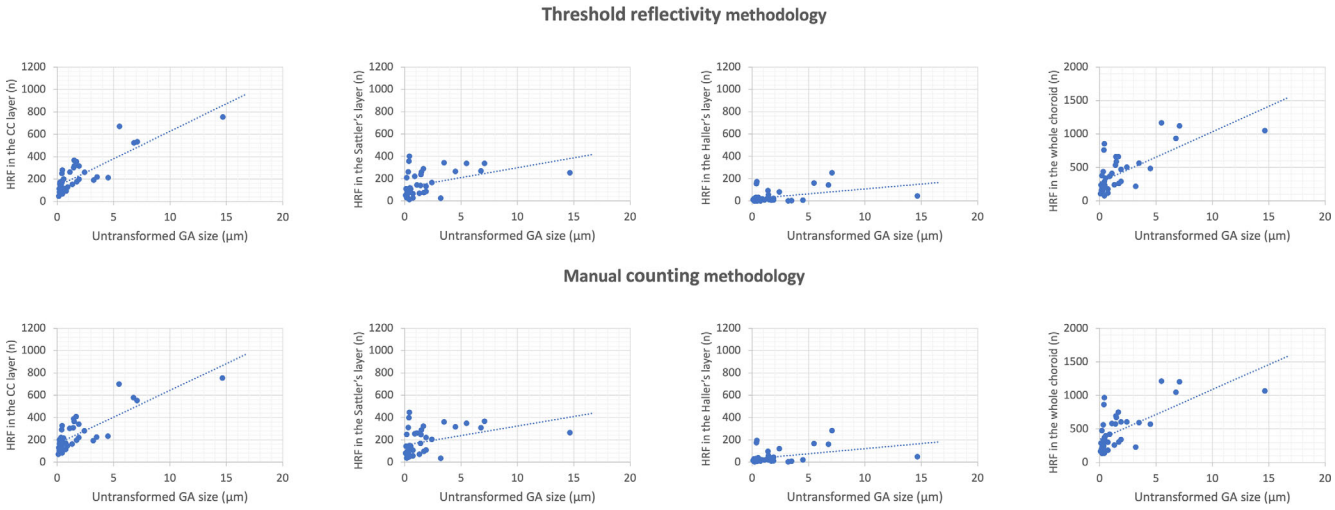

Figure 5. Scatterplots illustrating correlations between the number of choroidal hyperreflective foci (HRF) and the untransformed geographic atrophy (GA) size. (Upper scatterplots) Relationship between the untransformed GA size and average number of choroidal HRF obtained using the threshold reflectivity methodology in the choriocapillaris (CC; $\rho = 0.748$ and $P < 0.0001$ and CC; $\rho = 0.727$ and $P < 0.0001$), Sattler's ($\rho = 0.495$ and $P = 0.001$) ($\rho = 0.491$ and $P = 0.001$), and Haller's ($\rho = 0.386$ and $P = 0.014$) ($\rho = -0.351$ and $P = 0.026$) layers, and whole choroid ($\rho = 0.679$ and $P < 0.0001$) ($\rho = 0.672$ and $P < 0.0001$). (Lower scatterplots) Relationship between the untransformed GA size and average number of choroidal HRF obtained using the manual counting methodology in the CC ($\rho = 0.727$ and $P < 0.0001$), Sattler's ($\rho = 0.491$ and $P = 0.001$), and Haller's ($\rho = -0.351$ and $P = 0.026$) layers, and whole choroid ($\rho = 0.672$ and $P < 0.0001$).

Discussion

In this study, we described prevalence and characteristics of choroidal HRF in eyes with GA secondary to AMD. We observed that these eyes may be characterized by presence of choroidal HRF which are more prevalent in the CC and Sattler's layers. The reason for the occurrence of HRF in the choroid of patients with GA is uncertain and this has been thoroughly discussed in the following paragraphs. We may speculate that some choroidal HRF located at the level of Bruch's membrane may be the imaging surrogate of "dissociated" RPE cells previously displayed in histologic images of patients with AMD.[30] Nonetheless, considering that these choroidal HRF are not exclusive to GA in AMD and have been observed in other conditions characterized by RPE atrophy (i.e. Stargardt disease),[22] it is plausible to propose that they might actually be regular components of the choroid. Their visualization could be enhanced in GA eyes due to improved signal penetration resulting from the absence of RPE.

As mentioned above, choroidal HRF have been detected using structural OCT imaging in various disorders, including diabetic macular edema[21] and Stargardt disease.[22] In details, Roy and colleagues[21] retrospectively examined the presence of choroidal HRF in 119 eyes of 60 patients with diabetic macular edema. Using spectral domain OCT, they reported the presence of choroidal HRF in 59 eyes, which corresponds to 49.5% of the total sample size. The authors proposed a hypothesis that the choroidal HRF observed in diabetic macular edema may be caused by the migration of neuroretinal HRF into the choroid. This theory was based on the fact that all 59 eyes with choroidal HRF in the study also had neuroretinal HRF, whereas none of the eyes had choroidal HRF without neuroretinal HRF. In another study, Piri et al.[22] performed a retrospective analysis on 26 eyes of 13 patients with Stargardt disease. Using spectral domain OCT, the authors demonstrated the presence of choroidal HRF in all the examined cases. Notably, the authors demonstrated that there is a positive correlation between the number of HRF in the CC and the Sattler's layer and disease duration. In the latter study, the authors speculated that the presence of choroidal HRF in patients with Stargardt disease may suggest that lipofuscin deposits migrate from the outer retina to the choroid through a degradation process.[22]

We add to the literature by reporting the prevalence of choroidal HRF in eyes with GA and AMD, which were assessed using structural OCT. Moreover, we provided a qualitative and quantitative description of these findings. In our study cohort of 40 eyes with a diagnosis of GA, choroidal HRF were present in all the examined cases. Notably, choroidal HRF were mainly localized in the CC and Sattler's layers.

As mentioned above, neuroretinal HRF occurring in GA have been proposed to originate from activated RPE cells that migrate anteriorly within the retina.[16] Curcio et al.[31] give credence to the latter theory in a previous important histopathological study which correlated structural OCT findings to histology in donor eyes and showed that RPE cells on the druse apex either migrate into the retina or die, and the druse collapses, because the RPE is not present to maintain it. Within the atrophic zone, there may be scattered fully pigmented, nucleated cells known as "dissociated" RPE cells.[30] These cells can survive in regions with cRORA and may migrate to and flatten against Bruch's membrane (i.e. "subducted" cells).[30] Therefore, those choroidal HRF displayed at the level of Bruch's membrane might in part indicate the posterior migration of RPE cells.

Nevertheless, it is important to recognize that some choroidal HRF were observed without the presence of posterior shadowing, which is typically associated with HRF caused by migrating RPE cells.[31] Moreover, as mentioned above, Curcio and colleagues[30] were not able to display the presence of RPE cells extending beyond Bruch's membrane,

whereas some of the choroidal HRF visualized on structural OCT are located in between major choroidal vessels.

We indeed observed HRF in the choroidal stroma, which is the connective tissue surrounding the vessels of the choroid. This stroma contains various components, including neurons and nerve processes, melanocytes, inflammatory cells (e.g. mast cells), and extracellular matrix components.[32] Assuming that there is a lack of evidence that RPE cells may migrate beyond Bruch's membrane, some choroidal HRF may be associated with the presence of these components, whose visualization might be ameliorated in GA eyes because of the increased signal penetration due to the absent RPE. The latter hypothesis gains additional support from the observation that these choroidal HRF are not exclusive to GA in AMD. We did indeed observe these OCT features within the choroid of patients with intermediate AMD. Moreover, they have been previously identified in other conditions marked by RPE degeneration (i.e. Stargardt disease).[22]

Our study had two primary limitations. First, we did not conduct any correlation analyses between the imaging and histologic findings, which is an important aspect that needs to be explored in future research to determine the underlying mechanisms and implications of this phenomenon. Second, we used spectral domain OCT scans without the enhanced depth imaging (EDI) technique, which could have potentially allowed for better visualization of the choroidal layers. However, it should be noted that EDI-OCT scans did not improve the visualization of choroidal HRF in Stargardt disease.[22] Finally, our research revealed a direct relationship between the number of choroidal HRF and the size of GA, indicating that cases with larger GA regions were characterized by a higher quantity of choroidal HRF. Nevertheless, as previously mentioned, this relationship might be a consequence of the larger GA size facilitating better identification of these choroidal abnormalities due to improved signal penetration caused by the absence of RPE. Consequently, this connection could be coincidental and would not necessarily indicate a link between disease severity and the quantity of choroidal HRF. One last limitation to consider is the homogeneity of our patient population, as all individuals in the study were of Caucasian ethnicity, and data on iris color were not available. In light of the hypothesis that choroidal HRF may be related to melanocytes, forthcoming research will help determine whether these factors impact the presence and quantity of choroidal HRF.

In conclusion, this OCT study demonstrates that HRF may be visualized in the choroid of patients with GA. These HRF are mainly located in the CC and Sattler's layers. Future studies providing correlations between histology and imaging will provide a better understanding of the underlying mechanisms involved in the formation/visualization of choroidal HRF. Additionally, future research utilizing longitudinal data could shed light on whether choroidal HRF modify over time and whether their presence and quantity are linked to disease status and growth patterns. Ultimately, forthcoming research endeavors may shed light on whether these choroidal HRF are prevalent across various forms of RPE atrophy, thanks to enhanced signal penetration resulting from the RPE's absence.

Acknowledgments

Disclosure: **E. Borrelli**, AbbVie (C), Bayer (C), Roche (C), Zeiss (C); **M. Reibaldi**, AbbVie (C), Bayer (C), Roche (C), Novartis (C); **C. Barresi**, None; **A. Berni**, None; **U. Introini**, None; **F. Bandello**, AbbVie (C), Alimera (C), Bayer (C), Boehringer-Ingelheim (C), Fidia Sooft (C), Hofmann La Roche (C), Novartis (C), Ntc Pharma (C), Oxurion Nv (C), Sifi (C)

References

1. Ferris FL, Wilkinson CP, Bird A, et al. Clinical classification of age-related macular degeneration. *Ophthalmology*. 2013;120(4):844–851.
2. Rudnicka AR, Kapetanakis VV, Jarrar Z, et al. Incidence of late-stage age-related macular degeneration in American Whites: systematic review and meta-analysis. *Am J Ophthalmol*. 2015;160(1):85–93.e3.
3. Klein R, Klein BEK, Linton KLP. Prevalence of age-related maculopathy: the Beaver Dam Eye study. *Ophthalmology*. 2020;127(4S):S122–S132.
4. Dolz-Marco R, Balaratnasingam C, Messinger JD, et al. The border of macular atrophy in age-related macular degeneration: a clinicopathologic correlation. *Am J Ophthalmol*. 2018;193:166–177.
5. Chu Z, Shi Y, Zhou X, et al. Optical coherence tomography measurements of the retinal pigment epithelium to Bruch membrane thickness around geographic atrophy correlate with growth. *Am J Ophthalmol*. 2022;236:249–260.
6. Marsiglia M, Boddu S, Bearelly S, et al. Association between geographic atrophy progression and reticular pseudodrusen in eyes with dry age-related macular degeneration. *Invest Ophthalmol Vis Sci*. 2013;54(12):7362–7369.
7. Niu S, de Sisternes L, Chen Q, Rubin DL, Leng T. Fully automated prediction of geographic atrophy growth using quantitative spectral-domain optical coherence tomography biomarkers. *Ophthalmology*. 2016;123(8):1737–1750.
8. Veerappan M, El-Hage-Sleiman AKM, Tai V, et al. Optical coherence tomography reflective drusen substructures predict progression to geographic atrophy in age-related macular degeneration. *Ophthalmology*. 2016;123(12):2554–2570.
9. Shi Y, Zhang Q, Zhou H, et al. Correlations between choriocapillaris and choroidal measurements and the growth of geographic atrophy using swept source OCT imaging. *Am J Ophthalmol*. 2021;224:321–331.
10. Zhang Q, Shi Y, Shen M, et al. Does the outer retinal thickness around geographic atrophy represent another clinical biomarker for predicting growth? *Am J Ophthalmol*. 2022;244:79–87.
11. Hirabayashi K, Yu HJ, Wakatsuki Y, Marion KM, Wykoff CC, Sadda SR. OCT risk factors for development of atrophy in eyes with intermediate age-related macular degeneration. *Ophthalmol Retina*. 2023;7(3):253–260.
12. Coscas G, De Benedetto U, Coscas F, et al. Hyperreflective dots: a new spectral-domain optical coherence tomography entity for follow-up and prognosis in exudative age-related macular degeneration. *Ophthalmologica*. 2013;229(1):32–37.
13. Nassisi M, Lei J, Abdelfattah NS, et al. OCT risk factors for development of late age-related macular degeneration in the fellow eyes of patients enrolled in the HARBOR study. *Ophthalmology*. 2019;126(12):1667–1674.
14. Nassisi M, Fan W, Shi Y, et al. Quantity of intraretinal hyperreflective foci in patients with intermediate age-related macular degeneration correlates with 1-year progression. *Invest Ophthalmol Vis Sci*. 2018;59(8):3431–3439.
15. Borrelli E, Zuccaro B, Zucchiatti I, et al. Optical coherence tomography parameters as predictors of treatment response to eplerenone in central serous chorioretinopathy. *J Clin Med*. 2019;8(9):1271.
16. Zanzottera EC, Ach T, Huisingh C, Messinger JD, Spaide RF, Curcio CA. Visualizing retinal pigment epithelium pheno-

types in the transition to geographic atrophy in age-related macular degeneration. *Retina*. 2016;36(Suppl. 1):S12–S25.

17. Augustin S, Lam M, Lavalette S, et al. Melanophages give rise to hyperreflective foci in AMD, a disease-progression marker. *J Neuroinflammation*. 2023;20(1):28.
18. Sacconi R, Sarraf D, Garrity S, et al. Nascent type 3 neovascularization in age-related macular degeneration. *Ophthalmol Retina*. 2018;2(11):1097–1106.
19. Christenbury JG, Folgar FA, O'Connell R V, Chiu SJ, Farsiu S, Toth CA. Progression of intermediate age-related macular degeneration with proliferation and inner retinal migration of hyperreflective foci. *Ophthalmology*. 2013;120(5):1038–1045.
20. Schmidt-Erfurth U, Bogunovic H, Grechenig C, et al. Role of deep learning-quantified hyperreflective foci for the prediction of geographic atrophy progression. *Am J Ophthalmol*. 2020;216:257–270.
21. Roy R, Saurabh K, Shah D, Chowdhury M, Goel S. Choroidal hyperreflective foci: a novel spectral domain optical coherence tomography biomarker in eyes with diabetic macular edema. *Asia Pac J Ophthalmol (Phila)*. 2019;8(4):314–318.
22. Piri N, Nesmith BLW, Schaal S. Choroidal hyperreflective foci in Stargardt disease shown by spectral-domain optical coherence tomography imaging: correlation with disease severity. *JAMA Ophthalmol*. 2015;133(4):398–405.
23. Schmitz-Valckenberg S, Sahel JA, Danis R, et al. Natural history of geographic atrophy progression secondary to age-related macular degeneration (Geographic Atrophy Progression Study). *Ophthalmology*. 2016;123(2):361–368.
24. Huang Y, Gangaputra S, Lee KE, et al. Signal quality assessment of retinal optical coherence tomography images. *Invest Ophthalmol Vis Sci*. 2012;53(4):2133–2141.
25. Borrelli E, Uji A, Sarraf D, Sadda SR. Alterations in the choriocapillaris in intermediate age-related macular degeneration. *Invest Opthalmol Vis Sci*. 2017;[in press](11):4792–4798.
26. Zhao J, Wang YX, Zhang Q, Bin Wei W, Xu L, Jonas JB. Macular choroidal small-vessel layer, Sattler's layer and Haller's layer thicknesses: the Beijing Eye Study. *Sci Rep*. 2018;8(1):4411.
27. Dolz-Marco R, Gal-Or O, Freund KB. Choroidal thickness influences near-infrared reflectance intensity in eyes with geographic atrophy due to age-related macular degeneration. *Invest Opthalmol Vis Sci*. 2016;57(14):6440.
28. Abdelfattah NS, Sadda J, Wang Z, Hu Z, Sadda S. Near-infrared reflectance imaging for quantification of atrophy associated with age-related macular degeneration. *Am J Ophthalmol*. 2020;212:169–174.
29. Sadda SR, Guymer R, Holz FG, et al. Consensus definition for atrophy associated with age-related macular degeneration on OCT: classification of atrophy report 3. *Ophthalmology*. 2018;125(4):537–548.
30. Cao D, Leong B, Messinger JD, et al. Hyperreflective foci, optical coherence tomography progression indicators in age-related macular degeneration, include transdifferentiated retinal pigment epithelium. *Invest Ophthalmol Vis Sci*. 2021;62(10):34.
31. Curcio CA, Zanzottera EC, Ach T, Balaratnasingam C, Freund KB. Activated retinal pigment epithelium, an optical coherence tomography biomarker for progression in age-related macular degeneration. *Invest Ophthalmol Vis Sci*. 2017;58(6):BIO211–BIO226.
32. Borrelli E, Sarraf D, Freund KB, Sadda SR. OCT angiography and evaluation of the choroid and choroidal vascular disorders. *Prog Retin Eye Res*. 2018;67:30–55.